

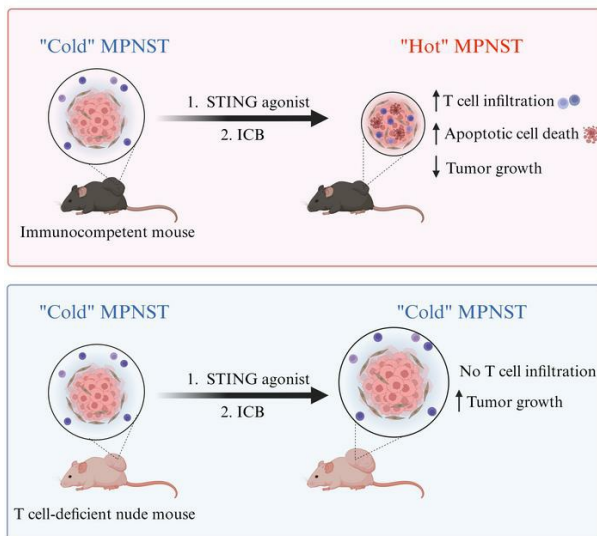
STING activation reprograms the microenvironment to sensitize NF1-related malignant peripheral nerve sheath tumors for immunotherapy

Bandarigoda N. Somatilaka, ... , Renee M. McKay, Lu Q. Le

J Clin Invest. 2024. <https://doi.org/10.1172/JCI176748>.

Research In-Press Preview Oncology Therapeutics

Graphical abstract



Find the latest version:

<https://jci.me/176748/pdf>



STING Activation Reprograms the Microenvironment to Sensitize NF1-related Malignant Peripheral Nerve Sheath Tumors for Immunotherapy

Bandarigoda N. Somatilaka¹, Laasya Madana¹, Ali Sadek¹, Zhiguo Chen¹, Sanjay Chandrasekaran^{2,3}, Renee M. McKay¹, and Lu Q. Le^{1,2,4,5,6,7}

¹Department of Dermatology, ²Simmons Comprehensive Cancer Center, ³Department of Internal Medicine, Division of Hematology/Oncology, ⁴UTSW Comprehensive Neurofibromatosis Clinic, ⁵Hamon Center for Regenerative Science and Medicine, ⁶O'Donnell Brain Institute, University of Texas Southwestern Medical Center at Dallas, Dallas, Texas, 75390-9069, USA, ⁷Department of Dermatology, University of Virginia School of Medicine, Charlottesville, VA, 22903, USA

Author for correspondence:

Lu Q. Le, M.D., Ph.D.
Professor and Chair
Department of Dermatology
University of Virginia School of Medicine
Phone: (434) 982-5974
Fax: (434) 244-4504
E-mail: bkn6qd@uvahealth.org

Short title: Reprogramming MPNST for immune checkpoint blockade

Conflicts of interest: The authors have declared that they have no competing interests.

Keywords

Neurofibromatosis Type 1, NF1, neurofibroma, plexiform neurofibroma, malignant peripheral nerve sheath tumor, MPNST, STING, immune checkpoint blockade, ICB, ADU-S100

Abstract

Neurofibromatosis Type 1 (NF1) is caused by mutations in the *NF1* gene that encodes neurofibromin, a RAS GTPase-Activating Protein. Inactivating *NF1* mutations cause hyperactivation of RAS-mediated signaling, resulting in development of multiple neoplasms, including Malignant Peripheral Nerve Sheath Tumors (MPNSTs). MPNSTs are an aggressive tumor and the main cause of mortality in NF1 patients. MPNSTs are difficult to resect and refractory to chemo- and radiotherapy, and no molecular therapies currently exist. Immune Checkpoint Blockade (ICB) is an approach to treat inoperable, undruggable cancers like MPNST, but successful outcomes require an immune cell-rich tumor microenvironment (TME). While MPNSTs are non-inflamed “cold” tumors, here, we turned MPNSTs into T cell-inflamed “hot” tumors by activating “stimulator of interferon genes” (STING) signaling. Mouse genetic and human xenograft MPNST models treated with STING agonist plus ICB exhibited growth delay via increased apoptotic cell death. This strategy offers a potential treatment regimen for MPNST.

Introduction

Neurofibromatosis type 1 (NF1) affects 1 in 3,000 individuals. A hallmark feature of NF1 is the development of benign cutaneous and plexiform neurofibromas that arise in the skin and peripheral nerve plexuses, respectively. In up to 10% of NF1 patients, benign plexiform neurofibromas undergo transformation into malignant peripheral nerve sheath tumors (MPNSTs), which are highly aggressive and are the leading cause of death in NF1 patients (1).

NF1 is associated with inactivating mutations in the *NF1* gene that encodes neurofibromin, a RAS GTPase activating protein. Neurofibromin binds to the GTP-bound active form of RAS and enhances the GTPase activity, negatively regulating downstream signaling. As a result, inactivating mutations in *NF1* activate multiple effector cascades including the RAS/RAF/MEK/ERK and PI3K/AKT/mTOR pathways (2). Inhibition of RAS and RAS-activated downstream signaling pathways have been explored as treatments for MPNST, however, these efforts have been unsuccessful, yielding no significant improvement in MPNST patient survival in clinical trials (3-5). The MEK inhibitor, selumetinib, is currently the only FDA-approved drug for treatment of NF1-associated inoperable plexiform neurofibroma but it is not effective against MPNST (6-9). To date, pharmacologic targeting of dysregulated signaling pathways remains an unsuccessful strategy to treat MPNST. Surgical resection therefore remains the primary treatment for MPNST although achieving complete tumor removal is often challenging due to the large size of the tumor and/or proximity to nerves (10, 11). Additionally, MPNSTs often metastasize, and patients have a high tendency for relapse following tumor resection. MPNSTs are also refractory to chemotherapy and radiotherapy, leading to dismal survival rates for MPNST patients (12-15). Thus, new, effective treatment strategies for MPNST are desperately needed.

Cancer cells use a variety of mechanisms to escape destruction by the host immune system. One way is by hijacking immune checkpoint control mechanisms that serve to avoid collateral damage during a normal immune response. The Programmed Cell Death Protein 1 (PD-1) pathway limits T cell effector functions within tissues. By expressing its ligand PD-L1, tumor cells block T-cell-mediated antitumor immune responses in the tumor microenvironment (16). Immune checkpoint blockade (ICB) therapy is a strategy in cancer immunotherapy that disrupts these ligand-receptor interactions, reprogramming a patient's immune system to target inoperable, undruggable tumors (17) by inhibiting ligand-receptor interactions used by cancer cells to escape immune destruction. Use of monoclonal antibodies to disrupt the interaction between PD-1 and PD-L1 is a widely used ICB therapy, however, having a T cell-enriched tumor microenvironment is critical for ICB therapy success (17). Unfortunately, MPNSTs are non-T cell inflamed or "cold" tumors, and therefore not likely to elicit an anti-tumor immune response to checkpoint inhibition (18-20). It has been shown that some MPNSTs have more prevalent PD-L1 expression than normal nerves, benign neurofibromas, or schwannomas (19), while another study reported similar levels of PD-L1 expression in MPNST and benign NF1 related tumors (21). A more recent study showed that PD-L1 was significantly elevated in sera of NF1 patients with MPNSTs compared to NF1 patients without MPNSTs suggesting a positive correlation between PD-L1 expression and MPNST progression (22). Therefore, increasing intratumoral T cell density, along with immune checkpoint inhibitor treatment, could generate T cell-mediated anti-tumor responses in MPNST.

The discovery of how the cGAS-STING-IFN pathway augments antitumor immunity via enriching an immune-suppressive tumor microenvironment may lead to further breakthroughs in cancer immunotherapy (23, 24). Cyclic GMP-AMP synthase (cGAS) enzyme binds to naked double-stranded DNA and undergoes conformational changes that allow it to convert ATP and

GTP into 2'3'-cyclic GMP-AMP (cGAMP). cGAMP functions as a second messenger that binds to its ER-resident adaptor protein STING (stimulator of interferon genes). cGAMP binding induces a conformational change in STING that exposes the C-terminal tail for TANK-binding kinase 1 (TBK1) binding and activation. TBK1 phosphorylates Interferon Regulatory Factor 3 (IRF3), which induces type I interferons (IFNs). Type I IFNs bind to the type I IFN receptor, activating a signaling cascade leading to expression of IFN-stimulated genes. STING also activates Inhibitor of Nuclear Factor- κ B ($I\kappa$ B) kinase (IKK) and subsequently Nuclear Factor- κ B (NF κ B) for pro-inflammatory cytokine induction. Activation of the STING-IFN axis in tumor cells promotes anti-proliferative and immuno-modulatory activities including enhancing T cell infiltration into the tumor microenvironment (25, 26). Therefore, activation of the STING-IFN pathway could convert cold MPNSTs into hot tumors.

Here, we report that treatment of a genetic, spontaneous mouse MPNST model with a STING agonist converts the tumor microenvironment from cold to hot, as shown by the intratumoral infiltration of T cells. Treating this *in vivo* mouse model with both STING agonist and ICB resulted in apoptosis of tumor cells and inhibition of tumor growth. Further, STING activation followed by ICB caused a much accelerated complete regression of human tumors in a xenograft model of MPNST. These studies leveraging our preclinical MPNST models support testing the combination of STING agonist with ICB as a treatment strategy for NF1 patients with MPNST.

RESULTS

MPNSTs are cold tumors but do express PD-L1

A spontaneous mouse model of MPNST was generated by recombination of *Nf1* and *p53* null alleles in *cis* on chromosome 11 (27, 28). As a result of spontaneous loss of the wild-type *Nf1* and *p53* alleles, *cisNf1*^{+/-}; *p53*^{+/-} (hereafter referred to as *cisNP*) mice develop a variety of sarcomas including MPNST (*cis*MPNST) between 3-7 months of age. Human MPNSTs have been reported to be cold tumors lacking T cell infiltration (18, 19, 29). To confirm that the MPNSTs that develop in this *cisNP* mouse model are also non-inflamed tumors, we performed immunohistochemistry (IHC) with antibodies against various immune cell types. As has been reported for human MPNST, we found that *cis*MPNSTs contain few T cells (including CD3-positive T cells, CD4-positive T helper cells, and CD8 α -positive cytotoxic T cells) (Figure 1A) and few B cells (CD20) (Figure 1B) compared to spleen and plexiform neurofibroma (pNF). They express macrophages (Iba1), including less M1 macrophages (iNOS) and more M2 macrophages (mannose receptor) compared to pNF (Figure 1C). MPNSTs that develop in allograft mice, in which MPNST cells are harvested from *cisNP* mice and implanted into athymic nude mouse hosts, are also negative for CD3, CD4, and CD8 α expression (Figure 1A), which was expected and served as a control as nude mice do not have a normal immune system and lack T cells (30). Thus, *cis*MPNSTs are cold tumors lacking an inflamed tumor microenvironment.

PD-1 is usually expressed by immune cells to terminate an immune response and avoid collateral tissue damage (31). Therefore, a lack of PD-1 expression in *cis*MPNSTs would be consistent with the observed lack of T cell infiltration into the MPNST microenvironment. IHC for PD-1 expression confirmed that these tumors infrequently express PD-1 (Figure 1D). Interestingly, we found that like human MPNST, mouse *cis*MPNSTs contain PD-L1 expressing

cells (Figure 1D, Supplemental Figure 1A) thereby qualifying MPNST as a candidate for ICB targeting.

STING agonist treatment activates the STING pathway in MPNSTs

The cytosolic DNA sensing enzyme cGAS binds to double-stranded DNA and initiates a cascade of events leading to production of type I IFNs and pro-inflammatory cytokines and chemokines. This cytokine response presumably recruits immune cell infiltration into the tumor microenvironment. As such, a number of STING agonists have been developed for testing as potential immune boosters (32). Preclinical studies using mouse tumor models have assessed the efficacy of STING agonists in triggering the cGAS-STING-IFN axis and shown that these agonists increase innate immunity and produce a CD8+ T cell-rich environment (33-35). However, this approach has not been tested in MPNST.

We hypothesized that treating the *cisNP* MPNSTs with a STING agonist would result in the expression of cytokines and chemokines that would recruit T cells into the tumor. To test this, we used two different commercially available STING agonists - synthetic dinucleotide ADU-S100 (33-35) and synthetic non-nucleotide STING agonist 3 (SA3) (36). We first tested ADU-S100 on two different MPNST cell lines: mouse MPNST cell lines derived from *Nf1* and *p53* null skin progenitor cells (HTS-Luc MPNST) and *cis*MPNST cells derived from *cisNP* mice. Cells were treated for 8, 18, 24, or 48 hours and then harvested for western blot analysis, which showed increased expression of phospho-IRF and phospho-NFκB indicating STING pathway activation at 8 hours of ADU-S100 treatment (Supplemental Figure 1, B-C). qRT-PCR showed highest expression of cytokine/chemokine genes at 8 hours after ADU-S100 treatment (Supplemental

Figure 1D), showing that ADU-S100 treatment can activate STING-IFN signaling in MPNST cells.

We next tested STING agonists for activity in vivo: MPNSTs that developed in *cisNP* mice were injected either intratumorally with ADU-S100 or by intraperitoneal injection with SA3 and monitored for 12 days (Figure 2A, Supplemental Figure 2A, and Table 1). On day 12, the tumors were harvested and analyzed for activation of the STING pathway. We observed that markers of STING pathway activation, such as phospho-IRF3 and phospho-NFκB, were indeed upregulated in both the ADU-S100- and SA3-treated tumors compared to vehicle controls (Figure 2B and Supplemental Figure 2B), as were expression of proinflammatory cytokines/chemokines *Ifnb1*, *Tnf*, *Cxcl10*, and *Il12a* (Figure 2C and Supplemental Figure 2C). While the expression of some of the genes we analyzed showed a statistically significant increase upon ADU-S100 treatment, others were increased but without reaching statistical significance (Figure 2C). This could be because upregulation of STING signaling following STING agonist treatment is transient as evident from the in vitro experiments. As a result, our time of analysis - 5 days after the last treatment (day 12 of treatment scheme; Figure 2A) - could be too late to capture the more transitory changes in STING activation. To assess the temporal impact on cytokine expression, we harvested *cis*MPNSTs earlier, at 24 hours post-ADU-S100 treatment, and evaluated phospho-protein expression and target gene expression. At 24 hours, we saw statistically significant upregulation of STING signaling pathway (Figure 2 D-E).

STING activation promotes T cell infiltration into MPNST in vivo

To determine whether activation of the STING pathway by ADU-S100 or SA3 was sufficient to recruit T cells into the *cis*MPNST tumor microenvironment (TME), we performed IHC for T cell

markers. IHC revealed that treatment with the STING agonists increased infiltration of CD3+ T cells, CD4+ helper T cells, and CD8+ cytotoxic T cells, as well as PD-1-expressing cells, into the tumor (Figure 3, A and B and Supplemental Figure 2, D and E). The number of PD-L1-expressing cells, however, was unchanged (Figure 3, A and B and Supplemental Figure 2, D and E). IHC for B cell marker CD20 and M1 macrophage marker iNOS showed no increase in the presence of either of these immune cell types (Figure 3C).

Together, these data demonstrate that treatment with STING agonist activates the STING pathway in our *cisNP* mice and promotes T cell infiltration into the tumor, thus transforming cold MPNSTs into hot tumors.

STING activation by STING agonists impedes MPNST growth

To determine whether STING activation alone had any effect on MPNST growth, we monitored tumor growth of STING agonist-treated tumors compared to vehicle-treated tumors. We found that treatment with either ADU-S100 alone or SA3 alone resulted in slower tumor growth indicating that STING activation and subsequent recruitment of immune cells to the tumor can impede tumor growth (Figure 3, D and E and Supplemental Figure 2F). However, STING agonist treatment alone did not cause complete regression of tumors. Co-staining with antibodies against CD3 and PD-1 demonstrated that a subset of PD-1-expressing cells were indeed T cells (Figure 3F). Since the tumor cells express PD-L1 (Figure 1D, 3A and B, and Supplemental Figure 2, D and E), it was possible that interaction of PD-L1 with PD-1 expressed on infiltrating T cells could cause immune escape of the tumor cells leading to persistence of the tumor (16). T-cell intrinsic STING signaling has been shown to promote regulatory T cell induction (37). A recent report also showed that Foxp3-positive regulatory T cells are abundant in human MPNST (38). Therefore, we

investigated whether Foxp3-positive T cells were present in the *cis*MPNSTs (Supplemental Figure 3A and B). Compared to the wild-type mouse spleen, vehicle-treated *cis*MPNST showed few Foxp3-positive cells. This was unaltered upon ADU-S100 treatment (Supplemental Figure 3A). Furthermore, immunoblot analysis did not show a significant difference in Foxp3 protein levels between vehicle- and ADU-S100-treated tumors (Supplemental Figure 3B).

As a control, we generated *cis*MPNSTs in athymic nude mice by subcutaneously implanting tumors harvested from *cis*NP mice into athymic mice (Supplemental Figure 4A). These allograft *cis*MPNSTs in athymic mice continued to grow despite ADU-S100 treatment (Supplemental Figure 4, B and C), suggesting that the immune inflammation resulting from STING activation is mediated by T cells in the context of MPNST. Here, we confirmed that the STING pathway was activated 24 hours after ADU-S100 treatment to rule out the possibility of non-upregulation of the pathway resulting in tumors responding similarly in the two experimental groups (Supplemental Figure 4, D and E).

Due to the close proximity to the *NF1* gene, somatic *TP53* mutations are frequent in human MPNSTs (39) (40). While the *cis*NP model offers similarity to such human NF1-associated MPNSTs, it can also present complications to this study as it is reported that mutations in p53 can affect immune cell function (41). Therefore, to overcome potential limitations of the *cis*NP model, in parallel, we treated a different mouse MPNST model – *PLP-CreERT2; Nf1^{fl/fl}; p53^{fl/fl}* mice (hereafter referred to as conditional MPNST) - with ADU-S100 (Supplemental Figure 5A). In this model, *Nf1* and *p53* are conditionally deleted in Schwann cell precursors providing spatiotemporal control over MPNST generation. Once mice were one week old, we subcutaneously injected 4-hydroxytamoxifen (dissolved in 100% ETOH at 4 mg/mL, 40 µg per pup) to induce conditional deletion of *Nf1* and *p53*. We let tumors develop until they were at least 5mm in diameter and then

treated them with ADU-S100 or vehicle. As in the case of *cis*MPNST, growth of these tumors was significantly delayed upon ADU-S100 treatment but were not completely regressed (Supplemental Figure 5, B-C).

Combination treatment of *cis*NP mice with STING agonist plus ICB slows tumor growth, increases T cell infiltration, and promotes apoptosis in MPNST

Our finding that STING agonist treatment could stimulate infiltration of PD-1-expressing T cells into tumors in our MPNST model indicated that these tumors might now be responsive to ICB. We therefore tested whether ICB treatment together with STING agonist would have an inhibitory effect on tumor growth. Figures 4A and 4B show the treatment arms and the combination treatment protocol, respectively, for the treatment of *cis*NP mice with the STING agonist ADU-S100 plus anti-PD-1 antibody or anti-PD-L1 antibody. On day 12 following the start of treatment, tumors were measured, and the mice euthanized. Similarly, conditional MPNSTs were treated with the combination of STING agonist and ICB (Supplemental Figure 5A). In contrast to the *cis*NP mice, conditional MPNST bearing mice were kept alive until tumor volumes reached maximum limits or got ulcerated (in accordance with animal welfare guidelines). As a control, we also treated MPNST allografts in nude mice with the same combination treatment (Figure 4C). We found that tumors in *cis*NP mice treated with the combination of STING agonist plus ICB were smaller compared to vehicle-treated (Figure 4D-E, Supplemental Figure 6, A-D), but found no significant difference in tumor size in allograft nude mice treated with vehicle versus drug (Figure 4D-E). Conditional MPNSTs that received STING agonist plus ICB were significantly smaller than the controls (Supplemental Figure 5, B and C) and the mice lived longer than the controls. This observation suggests that the MPNST growth delay initiated by STING activation is mediated

through T cells. Indeed, IHC analysis of the tumors with a panel of T cell markers showed increased presence of T cells in the tumors that received drug treatment (Figure 5, A and B; Supplemental Figure 7A).

To further investigate the molecular mechanisms responsible for the tumor growth delay observed upon STING activation and ICB, we performed IHC for markers of cell proliferation and apoptosis. Cell proliferation as measured by phospho-histone H3 (pH3) levels showed no significant difference among treatment groups (Figure 5C and D). However, cell death, as measured by expression of apoptosis markers cleaved caspase 3 and cleaved PARP was significantly increased in tumors treated with ADU-S100 alone and with ADU-S100 plus ICB (Figure 5C and D; Supplemental Figure 7B). Interestingly, MPNSTs that received the combination treatment of ADU-S100 plus α PD-1 showed significantly increased apoptotic cell death compared to those that received ADU-S100 only (Figure 5C and D, Supplemental Figure 7B). This, together with the observation that ADU-S100 plus α PD-1 tumors were significantly smaller than α PD-1 alone treated tumors (Figure 4D and E; Supplemental Figure 5B and C) suggests that ICB further facilitates the MPNST growth delay exerted by STING activation.

We also wanted to investigate whether adding another checkpoint blocking antibody in addition to α PD-1 and α PD-L1 would result in further reduction of tumor volume. For this, we treated *cisNP* mice with α PD-1 and α CTLA-4 monoclonal antibody on days 1 and 4 in combination with ADU-S100 (Supplemental Figure 8A). As a control, another set of *cisNP* mice received only ADU-S100 and α CTLA-4 (Supplemental Figure 8A). After 12 days, neither combination of ADU-S100 plus α PD-1 and α CTLA-4 nor ADU-S100 plus α CTLA-4 treatments showed a significant difference in tumor volume compared to ADU-S100 alone or ADU-S100 plus α PD-1 treatments (Supplemental Figure 8B and C). Upon further investigation, we saw that CTLA-4 protein levels

were not markedly different between control and ADU-S100 treated *cis*MPNSTs, which may explain why CTLA-4 inhibition did not challenge *cis*MPNST growth (Supplemental Figure 8D).

STING activation and ICB accelerate complete regression of xenograft human MPNST

Although we observed mouse MPNST growth delay in response to STING activation alone or with the combination treatment with ICB, their effect on human MPNST is not known. Therefore, to investigate the possibility of achieving complete human tumor regression, we treated a xenograft MPNST mouse model with either ADU-S100 or ADU-S100 plus α PD-1 (Figure 6A). Wild-type immunocompetent mice will eventually reject the implanted human tissue. Indeed, as expected, subcutaneously transplanted human MPNSTs were eliminated within a month with vehicle treatment (Figure 6B). We reasoned that treatment with STING agonist together with ICB might hasten this rejection and might do so faster than STING agonist treatment alone. Interestingly, while vehicle-treated tumors continued to grow during a short period post implantation, ADU-S100 only and ADU-S100 plus α PD-1-treated tumors started shrinking soon after treatment (Figure 6B). ADU-S100 only and combination treated tumors maintained a significantly smaller volume compared to the vehicle-treated tumors. Importantly, by day 14, tumors that received the combination treatment were significantly smaller than tumors treated with ADU-S100 alone and completely regressed more quickly than their ADU-S100-treated counterparts (Figure 6B, Supplemental Figure 9, A and B). As expected, ADU-S100 only and ADU-S100 plus ICB-treated xenograft tumors showed significantly higher T cell infiltration and apoptotic cell death (Figure 6C and D). However, the same human MPNST fragments transplanted in nude mice continued to grow despite drug treatments; unlike in immunocompetent mice, the tumors in the control group were not rejected by immunodeficient nude mice suggesting a requirement for T cells to mediate

the anti-tumor effects observed (Supplemental Figure 9C). Furthermore, cell death marked by cleaved caspase 3 and cleaved PARP was not significantly different among the treatment groups in nude mice but significantly lower than that in the respective treatment group in wild-type mice (Supplemental Figure 9, D and E).

Our data demonstrate that STING activation followed by ICB is more effective than ADU-S100 alone at eliminating MPNST in vivo. These proof-of-principle experiments support clinical testing of this combination treatment in patients with inoperable MPNST.

Discussion

There are currently no effective drugs available for treatment of MPNSTs, aggressive tumors that are the leading cause of death in NF1 patients. ICB has revolutionized cancer treatment, offering durable response for tumors that are immune inflamed; however, many tumor types, including MPNSTs, are cold tumors lacking immune cell infiltration, and thus are not good candidates for ICB therapy. To overcome this problem, various strategies to convert cold tumors to hot are currently being explored. These strategies include using low doses of radiation, oncolytic viruses, and harnessing the innate immune system.

A couple of reports describing the use of viral treatments to boost immune infiltration in MPNST have recently been published. In 2021, Ghonime et al. reported that a multimodal oncolytic virus engineered to express EphrinA2, an antigen expressed by a variety of tumor types, was able to induce a robust immune therapeutic response in immune competent mouse models of glioma and MPNST (42). A more recent report demonstrated that viral treatment of MPNST has the ability to transform the immune-desert environment: Yan et al. used intratumoral delivery of inactivated modified vaccinia virus Ankara (MVA) to enhance immune infiltration into MPNSTs making them amenable to ICB (43).

In this report, we harnessed the power of the innate immune system to facilitate immune destruction of murine MPNST. We found that STING agonist treatment of MPNSTs caused activation of the STING pathway, upregulation of cytokines and chemokines, and infiltration of immune cells including T cells, into the tumor. Of note, we found that STING agonist alone was able to significantly slow MPNST growth in our *cisNP* mice. However, STING activation alone could not completely ablate the tumor. This is a phenomenon reported by others who have employed STING activation for tumor inflammation as well (26). In the case of MPNST, this could

be due to immune escape of the tumor as a result of PD-L1 expression by a subset of tumor cells and its interaction with PD-1 on immune cells. Consequently, we observed enhanced tumor growth delay and significantly increased apoptosis upon STING activation followed by ICB compared to STING activation alone. Nevertheless, our experiments with ADU-S100 and ADU-S100 plus ICB had to be concluded within 12 days: *cisNP* mice form aggressive MPNSTs that grow rapidly, and control animals (treated with vehicle only) had to be sacrificed due to the size of the tumors. Hence, we could neither follow the drug-treated tumors long enough to assess for complete regression, nor could we determine survival curves for these studies.

To circumvent this issue, we generated a xenograft MPNST model in which we subcutaneously transplanted human MPNST in immunocompetent wild-type mice. As we could carefully measure tumor growth, this provided a more manageable system to test our treatment regimens. Based on our data with the *cisNP* mice, STING agonist treatment (ADU-S100) followed by systemic PD-1 inhibition yielded the most beneficial results against MPNST growth. Therefore, we tested the efficacy of ADU-S100 alone versus ADU-S100 plus α PD-1 in this xenograft mouse model. As expected with an immunocompetent host, animals who received vehicle treatment only were able to completely eliminate the xenograft tumor over time due to rejection of the human tissue by the murine immune system. However, STING activation alone enhanced this immune destruction while STING activation followed by ICB further significantly accelerated it.

In this study, the STING agonist ADU-S100 was administered by intratumoral injection. Human MPNSTs are often located internally, with close proximity to complex nerve networks. Therefore, we used STING agonist 3 (SA3), administered intraperitoneally to assess the efficiency of a systemically delivered drug in activating STING pathway. SA3 showed promise by upregulating STING signaling, increasing T cell infiltration, and inhibiting MPNST growth in

cisNP mice. Moreover, human primary MPNSTs tend to metastasize. Therefore, exploring whether STING activation and ICB can prime the immune system to target metastatic lesions is of importance in extending these studies into a clinical setting.

We have shown that STING activation reprograms the tumor microenvironment to enhance T cell infiltration into MPNST and sensitize it to ICB. It is worth discussing how benign plexiform neurofibroma (pNF) might respond to STING activation compared to MPNST. T cells have been shown to be present in pNF and play a positive role in pNF development. Since pNF is a hamartoma with minimal genetic mutation compared to MPNST, T cells likely recognize it as “self” (44, 45). However, MPNSTs, which have more neoantigens resemble “non-self” to T cells that infiltrate following STING activation and therefore can be targeted for immune destruction (46). Thus, it is possible that STING activation while restraining MPNST, might promote pNF progression by increasing T cell infiltration.

Combination treatment with STING agonist plus immune checkpoint inhibitors is currently being tested in clinical trials for some cancers. ADU-S100 was evaluated in a phase I clinical trial of 47 patients with advanced/metastatic solid tumors or lymphomas, either alone or in combination with ipilimumab, an immune checkpoint inhibitor that targets CTLA-4 (NCT02675439). However, the trial was terminated due to lack of anti-tumor activity. Another Phase 1 clinical trial testing the safety and maximum tolerated dose of STING agonist TAK-500 alone or with pembrolizumab, a monoclonal antibody targeting PD-1, is currently recruiting patients with locally advanced or metastatic solid tumors, however MPNST is not one of the eligible tumor types (NCT05070247). Our preclinical data support the testing of STING agonist together with immune checkpoint inhibition in clinical trials for the treatment of inoperable MPNST.

Methods

Sex as a biological variable

Our study examined male and female humans and mice, and similar findings are reported for both sexes.

Mice

All animals in this study were handled according to protocols approved by the UT Southwestern Institutional Animal Care and Use Committee, and mouse colonies were maintained in a barrier facility at UT Southwestern. Mice were housed in standard cages that contained three to five mice per cage, with water and standard diet ad libitum and a 12-hour light/dark cycle. The *cisNP* mouse model has been previously described (27, 28).

Genotyping

To determine the genotypes of the genetically modified mice, a 1 mm piece of tail was clipped from pups less than 2 weeks of age. Genomic DNA was extracted from this piece by incubating for 1.5 hours at 95°C in 50 mM NaOH. DNA lysates were then neutralized at room temperature with 1 M Tris-HCl (pH 7). To genotype *cisNP* mice, the following primers were used: For *Nf1* allele: 5940 (5' GTA TTG AAT TGA AGC ACC TTT GTT TGG 3'), 5941 (5' GCG TGT TCG AAT TCG CCA ATG 3'), and 5942 (5' CTG CCC AAG GCT CCC CCA G 3') primers generated a 194 bp band for the wild type and a 340 bp band for the heterozygote. For *Tp53* allele: GT-P53-1 (5' TAT ACT CAG AGC CGG CCT 3'), GT-P53-2 (5' CAT TCA GGA CAT AGC GTT GG 3'), and GT-P53-3 (5' ACA GCG TGG TGG TAC CTT AT 3') primers produced a 430 bp band for the wild type and a 650 bp band for the heterozygote. To genotype conditional MPNST mice,

the following primers were used: For *Nf1^{ff}* allele: 15228 (5' ACC TCT CTA GCC TCA GGA ATG A 3'), 15229 (5' CTT CAG ACT GAT TGT TGT ACC TGA 3'), 15588 (5' TGA TTC CCA CTT TGT GGT TCT AAG 3'), primers generated a 480 bp band for the wild type and a 350 bp band for the mutant. For *p53^{ff}* allele: P53-i5F (5' GGG GAG TTG TCT TTC GTG TGA 3'), P53-i6F (5' TGT GCC GAA CAG GTG GAA TA 3'), P53-i7R (5' CTA ACC TAC CAC GCG CCT TC 3'), primers generated a 275 bp band for the wild type and a 314 bp band for the mutant. For *PLP-CreERT2* allele: PLP-Ex2F (5' CCT CGT ATG CGT ACC TGA CT 3'), Cre-R69 (5' TGT GCC GAA CAG GTG GAA TA 3'), PLP-In3R (5' CAT TAG ACC GCT ACC TGC CA 3'), primers generated a 526 bp band for the wild type and a 190 bp band for the mutant. The DNA sequences were amplified with 2XTaq RED Master Mix (Apex).

MPNST allografts and xenografts in mice

Allografts: Athymic nude mice were purchased from Charles River Laboratories (stock no. 553). They were subcutaneously injected with 5 million *cis*MPNST cells per injection site. Once the injected cells formed tumors measuring 5 mm in diameter, mice were treated with STING agonist(s) and/ or monoclonal anti-PD-1/PD-L1 antibodies as described below.

Xenografts: Surgically resected metastatic MPNST tissue was subcutaneously transplanted into nude mice to generate a xenograft model. Samples of these tumors were then transplanted subcutaneously into wild type mice to generate xenograft MPNST in immunocompetent mice.

Cell culture

H358 cells (generously shared by Kate O'Donnell lab of UT Southwestern) are KRAS mutant human lung cancer cells that express PD-L1 (47). S462 cells are human NF1-related MPNST cells

(SCC414, Sigma-Aldrich). The *cis*MPNST cell line was generated in the lab by harvesting tumors from *cis*MPNST mice. HTS-Luc MPNST cell line was reported before (48). Human and mouse MPNST cell lines were cultured in DMEM high glucose (R8756, Sigma) supplemented with 10% FBS (5628, Sigma), 1% sodium pyruvate (S8636, Sigma), GlutaMAX (35050079, Gibco) and 1% penicillin/ streptomycin (T4049). For STING agonist treatments, cells were seeded in 6-well plates at 3×10^5 cells/ well concentration and allowed to grow to 80% confluency. The cells were then treated with 10 μ m of ADU-S100 for 8, 18, 24, or 48 hours. Cells were then washed with PBS and harvested for qRT-PCR and immunoblots or fixed for immunofluorescence.

Reverse transcription and qRT-PCR

Tumor tissue samples were frozen in liquid nitrogen and pulverized while cold. Total RNA from these tissues and cultured MPNST cells were extracted using TRI reagent (T9424, ThermoFisher Scientific), and 1 μ g RNA was reverse transcribed with an iScript Select cDNA Synthesis Kit (1708897, BioRad). Primer sequences are listed in Supplemental Table 1. qRT-PCR reaction mixtures were prepared with iTaq Universal SYBR Green Supermix (172-5124, BioRad), and reactions were performed in QuantStudio™ 3 Real-Time PCR System (ThermoFisher Scientific). Ct values were normalized to the housekeeping gene *Gusb*.

Immunoblotting

Protein lysates from tumor tissue and cultured tumor cells were made using RIPA buffer (8990, ThermoFisher Scientific) containing protease and phosphatase inhibitors (88265 and A32959 respectively, ThermoFisher Scientific). The following antibodies were used for immunoblotting; STING (13647S, Cell Signaling), TBK1 (3504T, Cell Signaling), pTBK1 (s172) (5483T, Cell

Signaling), IRF3 (MA5-32348, Invitrogen), pIRF3 (4947S, Cell Signaling), NFkB (ab16502, Abcam), pNFkB (3033S, Cell Signaling), PD-L1 (ab213480, Abcam, 66248-1-Ig, Proteintech), GAPDH (SC-32233, Santa Cruz Biotechnology), Vinculin (4650S, Cell Signaling), Foxp3 (ab215206, Abcam), CTLA-4 (BE0164, BioXCell).

Immunohistochemistry (IHC) and immunofluorescence (IF)

Tumors were fixed in formalin for at least 48 hours, processed and embedded in paraffin blocks using a Citadel 2000 Wax Bath. Serial 5- μ m sections were prepared for IHC and IF. Paraffin sections were deparaffinized in xylene and re-hydrated using ethanol and water. Antigens were retrieved by citrate antigen retrieval buffer (pH 6.0) or TE buffer (pH 9.0). Sections were then blocked and incubated with primary and secondary antibodies using standard methods. The following antibodies were used for IHC: CD20 (BS-0080R, Bioss), CD3 (ab16669, Abcam), CD4 (ab183685, Abcam), CD8 α (PA5-81344), Iba1 (019-19741, Fisher), iNos (ab15323, Abcam), mannose receptor (ab64693, Abcam), phospho Histone H3 (ser10) (9701s, Cell Signaling), Cleaved Caspase 3 (9661S, Cell Signaling) and Cleaved PARP (9488S, Cell Signaling). For IF, paraffin sections were incubated with CD3 (ab16669, Abcam) and PD-1 (ab214421, Abcam; 66220-1-Ig, Proteintech) antibodies overnight at room temperature followed by incubation with the Goat anti-Rabbit IgG-Cy3 secondary antibody (Jackson ImmunoResearch). After staining, images were acquired with an Olympus IX73 microscope. For quantification, 3-5 different fields of each sample were imaged. These fields were selected randomly avoiding the tumor borders. The target cell type was counted using ImageJ Cell Counter extension, and the average number of cells per 1 mm² was calculated. It should be noted that in control treatments, some of the markers that were looked at were scarcely expressed. In this situation, the development reaction in IHC

was continued longer to capture a positive signal. However, this resulted in higher background staining. At image acquisition, the same parameters were maintained for all tumor samples, regardless of the treatments. This resulted in some of the images from “control” sections having higher background (e.g. Figure 3A, PD-1). Similar high background staining was also observed in the control sections in IF images (e.g. Figure 3F), as CD3 and PD-1 positive cells were scarce in those sections.

STING agonist treatment and immune checkpoint blocking (ICB)

When *cisNP* mice or conditional MPNST-bearing mice or athymic mice with *cis*MPNST allografts developed a tumor with at least one dimension reaching 5 mm, they were treated with intratumoral (IT) injections of 50 µg of STING agonist ADU-S100 (HY-12885B, MedChemExpress). The day of the first injection was considered as day 1 and the injections were repeated on days 4 and 7. Each day the tumor(s) was measured at 3 perpendicular planes designated as length (L), width (W), and depth (D) and the tumor volume was calculated as $(L \times W \times D)/2$. On day 12, mice were sacrificed, and the tumors were harvested (Figure 2A, Figure 4B and C, S5A and D). For the welfare of the mice, the tumors were not allowed to grow more than 2 cm in diameter. Therefore, the length of the experiments was determined from results of pilot studies, based on the time that vehicle-treated tumors took to reach 2 cm in diameter. For the human xenograft tumor studies, 50 µg of ADU-S100 or 50 µg of ADU-S100 with 250 µg of mouse monoclonal anti PD-1 antibody (BE0146, BioXCell) were injected intratumorally on day 8. Alternatively, mice that were treated with STING Agonist 3 (SA3, HY-103665, MedChemExpress) received a single intraperitoneal (IP) injection of 50 mg/kg body weight and were sacrificed on day 12. To combine STING activation with ICB, IP injections of 250 µg of mouse monoclonal anti PD-1 antibody (BE0146,

BioXCell) or 100 µg of mouse monoclonal anti PD-L1 antibody (BE0146, BioXCell), 300 µg of mouse monoclonal anti CTLA-4 antibody (BE0164, BioXCell) were given on days 1 and 4 in addition to STING agonists, and mice were euthanized on day 12. Dosing regimens are shown in Table 1.

Statistics

All data points shown in the figures resulted from biological replicates. The number of replicates are described in the figure legends. Unless otherwise stated in the figure legend, two-tailed t test was used to determine statistical significance.

Study Approvals

Animal care and use in this study were approved by the Institutional Animal Care and Use Committee at University of Texas Southwestern Medical Center. The use of de-identified human tissue was approved by the IRB of the University of Texas Southwestern Medical Center.

Data availability

All represented data are included in the “Supporting data values” XLS file and will be available from the corresponding author upon request.

Acknowledgments

We thank the members of the Le lab for helpful discussions. LQL held a Career Award for Medical Scientists from the Burroughs Wellcome Fund and is the Thomas L. Shield, M.D. and Kenneth E. Greer, M.D. endowed Professor in Dermatology. This work is supported by funding from the U.S.

Department of Defense (W81XWH-22-1-0356), the National Cancer Institute of the NIH (R01 CA166593, the Developmental and Hyperactive RAS Tumor SPORE U54 CA196519), and the Elisabeth Reed Wagner Fund for Research and Clinical Care in Neurofibromatosis and Cardiothoracic Surgery. BNS is a Young Investigator Awardee from the Children's Tumor Foundation (2022-01-008).

Author Contributions:

Conceptualization, B.N.S., R.M.M., L.Q.L.; Investigation, B.N.S., S.C., A.S., L.M., Z.C.; Writing – original draft, B.N.S., R.M.M.; Writing – review and editing, all authors; Supervision and funding, L.Q.L.

References

1. Kim A, Stewart DR, Reilly KM, Viskochil D, Miettinen MM, and Widemann BC. Malignant Peripheral Nerve Sheath Tumors State of the Science: Leveraging Clinical and Biological Insights into Effective Therapies. *Sarcoma*. 2017;2017:7429697.
2. Ratner N, and Miller SJ. A RASopathy gene commonly mutated in cancer: the neurofibromatosis type 1 tumour suppressor. *Nat Rev Cancer*. 2015;15(5):290-301.
3. Kim A, Lu Y, Okuno SH, Reinke D, Maertens O, Perentesis J, et al. Targeting Refractory Sarcomas and Malignant Peripheral Nerve Sheath Tumors in a Phase I/II Study of Sirolimus in Combination with Ganetespib (SARC023). *Sarcoma*. 2020;2020:5784876.
4. Schuetze SM, Wathen JK, Lucas DR, Choy E, Samuels BL, Staddon AP, et al. SARC009: Phase 2 study of dasatinib in patients with previously treated, high-grade, advanced sarcoma. *Cancer*. 2016;122(6):868-74.
5. Chugh R, Wathen JK, Maki RG, Benjamin RS, Patel SR, Meyers PA, et al. Phase II multicenter trial of imatinib in 10 histologic subtypes of sarcoma using a bayesian hierarchical statistical model. *J Clin Oncol*. 2009;27(19):3148-53.
6. Gross AM, Wolters PL, Dombi E, Baldwin A, Whitcomb P, Fisher MJ, et al. Selumetinib in Children with Inoperable Plexiform Neurofibromas. *N Engl J Med*. 2020;382(15):1430-42.
7. Dombi E, Baldwin A, Marcus LJ, Fisher MJ, Weiss B, Kim A, et al. Activity of Selumetinib in Neurofibromatosis Type 1-Related Plexiform Neurofibromas. *N Engl J Med*. 2016;375(26):2550-60.

8. Jessen WJ, Miller SJ, Jousma E, Wu J, Rizvi TA, Brundage ME, et al. MEK inhibition exhibits efficacy in human and mouse neurofibromatosis tumors. *J Clin Invest.* 2013;123(1):340-7.
9. Markham A, and Keam SJ. Selumetinib: First Approval. *Drugs.* 2020;80(9):931-7.
10. Dunn GP, Spiliopoulos K, Plotkin SR, Hornicek FJ, Harmon DC, Delaney TF, et al. Role of resection of malignant peripheral nerve sheath tumors in patients with neurofibromatosis type 1. *J Neurosurg.* 2013;118(1):142-8.
11. Gachiani J, Kim D, Nelson A, and Kline D. Surgical management of malignant peripheral nerve sheath tumors. *Neurosurg Focus.* 2007;22(6):E13.
12. Yang JC, Chang AE, Baker AR, Sindelar WF, Danforth DN, Topalian SL, et al. Randomized prospective study of the benefit of adjuvant radiation therapy in the treatment of soft tissue sarcomas of the extremity. *J Clin Oncol.* 1998;16(1):197-203.
13. Kahn J, Gillespie A, Tsokos M, Ondos J, Dombi E, Camphausen K, et al. Radiation therapy in management of sporadic and neurofibromatosis type 1-associated malignant peripheral nerve sheath tumors. *Front Oncol.* 2014;4:324.
14. Chou D, Bilsky MH, Luzzati A, Fisher CG, Gokaslan ZL, Rhines LD, et al. Malignant peripheral nerve sheath tumors of the spine: results of surgical management from a multicenter study. *J Neurosurg Spine.* 2017;26(3):291-8.
15. Higham CS, Steinberg SM, Dombi E, Perry A, Helman LJ, Schuetze SM, et al. SARC006: Phase II Trial of Chemotherapy in Sporadic and Neurofibromatosis Type 1 Associated Chemotherapy-Naive Malignant Peripheral Nerve Sheath Tumors. *Sarcoma.* 2017;2017:8685638.

16. Okazaki T, and Honjo T. The PD-1-PD-L pathway in immunological tolerance. *Trends Immunol.* 2006;27(4):195-201.
17. Sharma P, and Allison JP. Dissecting the mechanisms of immune checkpoint therapy. *Nat Rev Immunol.* 2020;20(2):75-6.
18. Lee PR, Cohen JE, Tendi EA, Farrer R, GH DEV, Becker KG, et al. Transcriptional profiling in an MPNST-derived cell line and normal human Schwann cells. *Neuron Glia Biol.* 2004;1(2):135-47.
19. Shurell E, Singh AS, Crompton JG, Jensen S, Li YF, Dry S, et al. Characterizing the immune microenvironment of malignant peripheral nerve sheath tumor by PD-L1 expression and presence of CD8+tumor infiltrating lymphocytes. *Oncotarget.* 2016;7(39):64300-8.
20. Sharma S, Shah JS, and Bali H. Malignant peripheral nerve sheath tumor: A rare malignancy. *J Oral Maxillofac Pathol.* 2020;24(Suppl 1):S86-S90.
21. Haworth KB, Arnold MA, Pierson CR, Choi K, Yeager ND, Ratner N, et al. Immune profiling of NF1-associated tumors reveals histologic subtype distinctions and heterogeneity: implications for immunotherapy. *Oncotarget.* 2017;8(47):82037-48.
22. Farschtschi S, Kluwe L, Park SJ, Oh SJ, Mah N, Mautner VF, et al. Upregulated immunomodulator PD-L1 in malignant peripheral nerve sheath tumors provides a potential biomarker and a therapeutic target. *Cancer Immunol Immunother.* 2020;69(7):1307-13.
23. Cai X, Chiu YH, and Chen ZJ. The cGAS-cGAMP-STING pathway of cytosolic DNA sensing and signaling. *Mol Cell.* 2014;54(2):289-96.
24. Chen Q, Sun L, and Chen ZJ. Regulation and function of the cGAS-STING pathway of cytosolic DNA sensing. *Nat Immunol.* 2016;17(10):1142-9.

25. Wang-Bishop L, Wehbe M, Shae D, James J, Hacker BC, Garland K, et al. Potent STING activation stimulates immunogenic cell death to enhance antitumor immunity in neuroblastoma. *J Immunother Cancer*. 2020;8(1).
26. Jneid B, Bochnakian A, Hoffmann C, Delisle F, Djacoto E, Sirven P, et al. Selective STING stimulation in dendritic cells primes antitumor T cell responses. *Sci Immunol*. 2023;8(79):eabn6612.
27. Cichowski K, Shih TS, Schmitt E, Santiago S, Reilly K, McLaughlin ME, et al. Mouse models of tumor development in neurofibromatosis type 1. *Science*. 1999;286(5447):2172-6.
28. Vogel KS, Klesse LJ, Velasco-Miguel S, Meyers K, Rushing EJ, and Parada LF. Mouse tumor model for neurofibromatosis type 1. *Science*. 1999;286(5447):2176-9.
29. Lee PR, Cohen JE, and Fields RD. Immune system evasion by peripheral nerve sheath tumor. *Neurosci Lett*. 2006;397(1-2):126-9.
30. Pelleitier M, and Montplaisir S. The nude mouse: a model of deficient T-cell function. *Methods Achiev Exp Pathol*. 1975;7:149-66.
31. Wieder T, Eigentler T, Brenner E, and Rocken M. Immune checkpoint blockade therapy. *J Allergy Clin Immunol*. 2018;142(5):1403-14.
32. Amouzegar A, Chelvanambi M, Filderman JN, Storkus WJ, and Luke JJ. STING Agonists as Cancer Therapeutics. *Cancers (Basel)*. 2021;13(11).
33. Corrales L, Glickman LH, McWhirter SM, Kanne DB, Sivick KE, Katibah GE, et al. Direct Activation of STING in the Tumor Microenvironment Leads to Potent and Systemic Tumor Regression and Immunity. *Cell Rep*. 2015;11(7):1018-30.

34. Foote JB, Kok M, Leatherman JM, Armstrong TD, Marcinkowski BC, Ojalvo LS, et al. A STING Agonist Given with OX40 Receptor and PD-L1 Modulators Primes Immunity and Reduces Tumor Growth in Tolerized Mice. *Cancer Immunol Res.* 2017;5(6):468-79.
35. Sivick KE, Desbien AL, Glickman LH, Reiner GL, Corrales L, Surh NH, et al. Magnitude of Therapeutic STING Activation Determines CD8(+) T Cell-Mediated Anti-tumor Immunity. *Cell Rep.* 2018;25(11):3074-+.
36. Ning L, Wei W, Wenyang J, Rui X, and Qing G. Cytosolic DNA-STING-NLRP3 axis is involved in murine acute lung injury induced by lipopolysaccharide. *Clin Transl Med.* 2020;10(7):e228.
37. Ni H, Zhang H, Li L, Huang H, Guo H, Zhang L, et al. T cell-intrinsic STING signaling promotes regulatory T cell induction and immunosuppression by upregulating FOXP3 transcription in cervical cancer. *J Immunother Cancer.* 2022;10(9).
38. Mitchell DK, Burgess B, White E, Smith AE, Sierra Potchanant EA, Mang H, et al. Spatial gene expression profiling unveils immuno-oncogenic programs of NF1-associated peripheral nerve sheath tumor progression. *Clin Cancer Res.* 2023.
39. Legius E, Dierick H, Wu R, Hall BK, Marynen P, Cassiman JJ, et al. TP53 mutations are frequent in malignant NF1 tumors. *Genes Chromosomes Cancer.* 1994;10(4):250-5.
40. Greenblatt MS, Bennett WP, Hollstein M, and Harris CC. Mutations in the p53 tumor suppressor gene: clues to cancer etiology and molecular pathogenesis. *Cancer Res.* 1994;54(18):4855-78.
41. Munoz-Fontela C, Mandinova A, Aaronson SA, and Lee SW. Emerging roles of p53 and other tumour-suppressor genes in immune regulation. *Nat Rev Immunol.* 2016;16(12):741-50.

42. Ghonime MG, Saini U, Kelly MC, Roth JC, Wang PY, Chen CY, et al. Eliciting an immune-mediated antitumor response through oncolytic herpes simplex virus-based shared antigen expression in tumors resistant to viroimmunotherapy. *J Immunother Cancer*. 2021;9(10).
43. Yan J, Chen Y, Patel AJ, Warda S, Lee CJ, Nixon BG, et al. Tumor-intrinsic PRC2 inactivation drives a context-dependent immune-desert microenvironment and is sensitized by immunogenic viruses. *J Clin Invest*. 2022;132(17).
44. Fletcher JS, Pundavela J, and Ratner N. After Nf1 loss in Schwann cells, inflammation drives neurofibroma formation. *Neurooncol Adv*. 2020;2(Suppl 1):i23-i32.
45. Kershner LJ, Choi K, Wu J, Zhang X, Perrino M, Salomonis N, et al. Multiple Nf1 Schwann cell populations reprogram the plexiform neurofibroma tumor microenvironment. *JCI Insight*. 2022;7(18).
46. Magallon-Lorenz M, Terribas E, Ortega-Bertran S, Creus-Bachiller E, Fernandez M, Requena G, et al. Deep genomic analysis of malignant peripheral nerve sheath tumor cell lines challenges current malignant peripheral nerve sheath tumor diagnosis. *iScience*. 2023;26(2):106096.
47. Yu W, Hua Y, Qiu H, Hao J, Zou K, Li Z, et al. PD-L1 promotes tumor growth and progression by activating WIP and beta-catenin signaling pathways and predicts poor prognosis in lung cancer. *Cell Death Dis*. 2020;11(7):506.
48. Chau V, Lim SK, Mo W, Liu C, Patel AJ, McKay RM, et al. Preclinical therapeutic efficacy of a novel pharmacologic inducer of apoptosis in malignant peripheral nerve sheath tumors. *Cancer Res*. 2014;74(2):586-97.

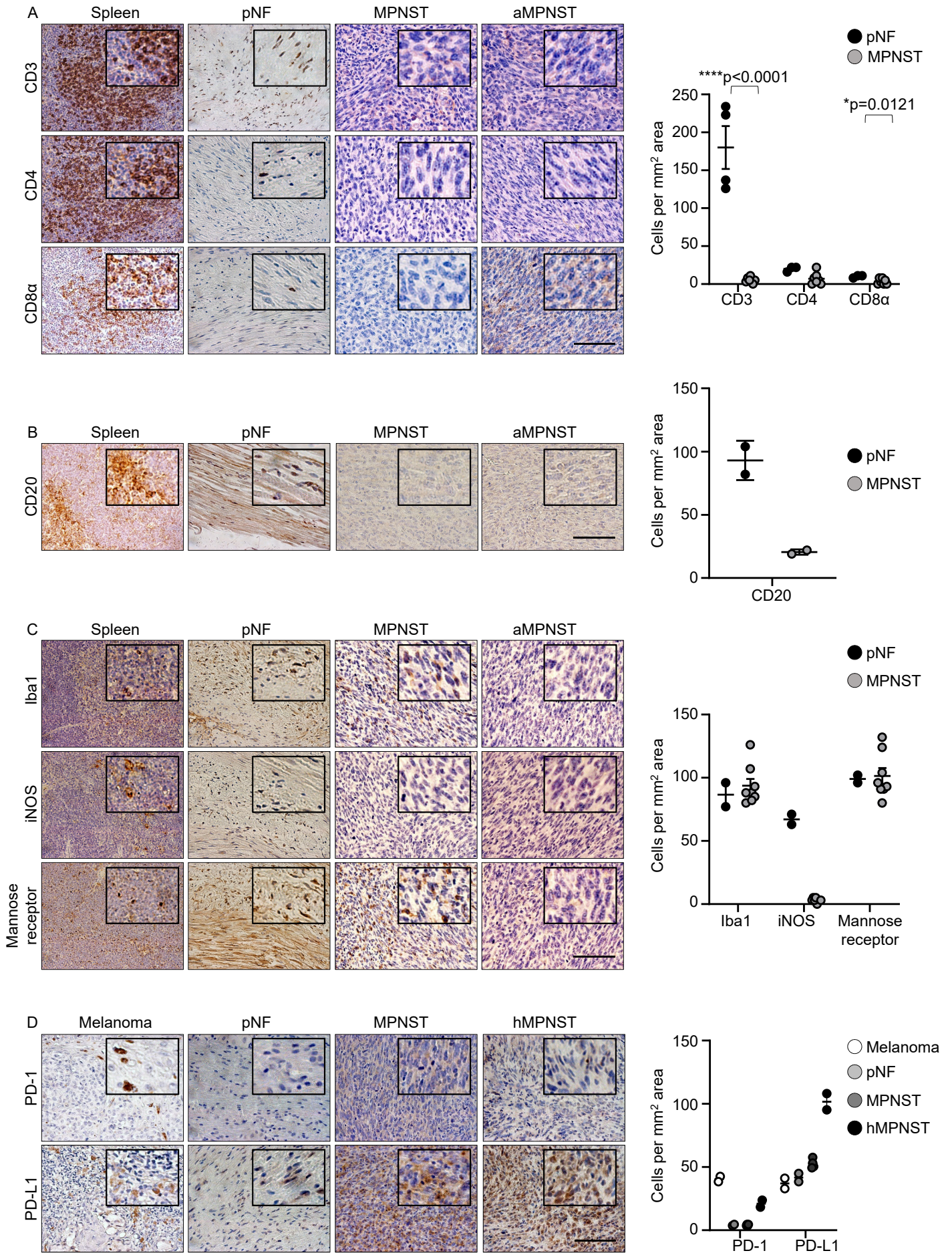


Figure 1. Characterization of the immune microenvironment of MPNST.

(**A-D**) Paraffin sections of murine spleen, murine plexiform neurofibroma (pNF) (harvested from *Sox10-CreERT*; *Nf1^{fl/fl}* mice induced with tamoxifen), murine MPNST (from *cisNP* mice), and MPNST allografts in athymic nude mice (aMPNST) were stained with antibodies against CD3, CD4, and CD8 α (**A**); CD20 (**B**); and Iba1, iNOS, and mannose receptor (**C**). (**D**) Paraffin sections of human melanoma, murine pNF, murine MPNSTs, and human MPNST (hMPNST) were stained with antibodies against PD-1 and PD-L1. Sections in (**A-D**) were counterstained with hematoxylin (blue) and the respective cell counts for (**A-D**) are shown on the right. Data are represented as mean \pm SEM and p values are determined by two-tailed t test with respect to pNF in (A), * $P < 0.05$, **** $P < 0.0001$. In (B-D) error bars indicate mean \pm SD. Scale bar: 50 μ m.

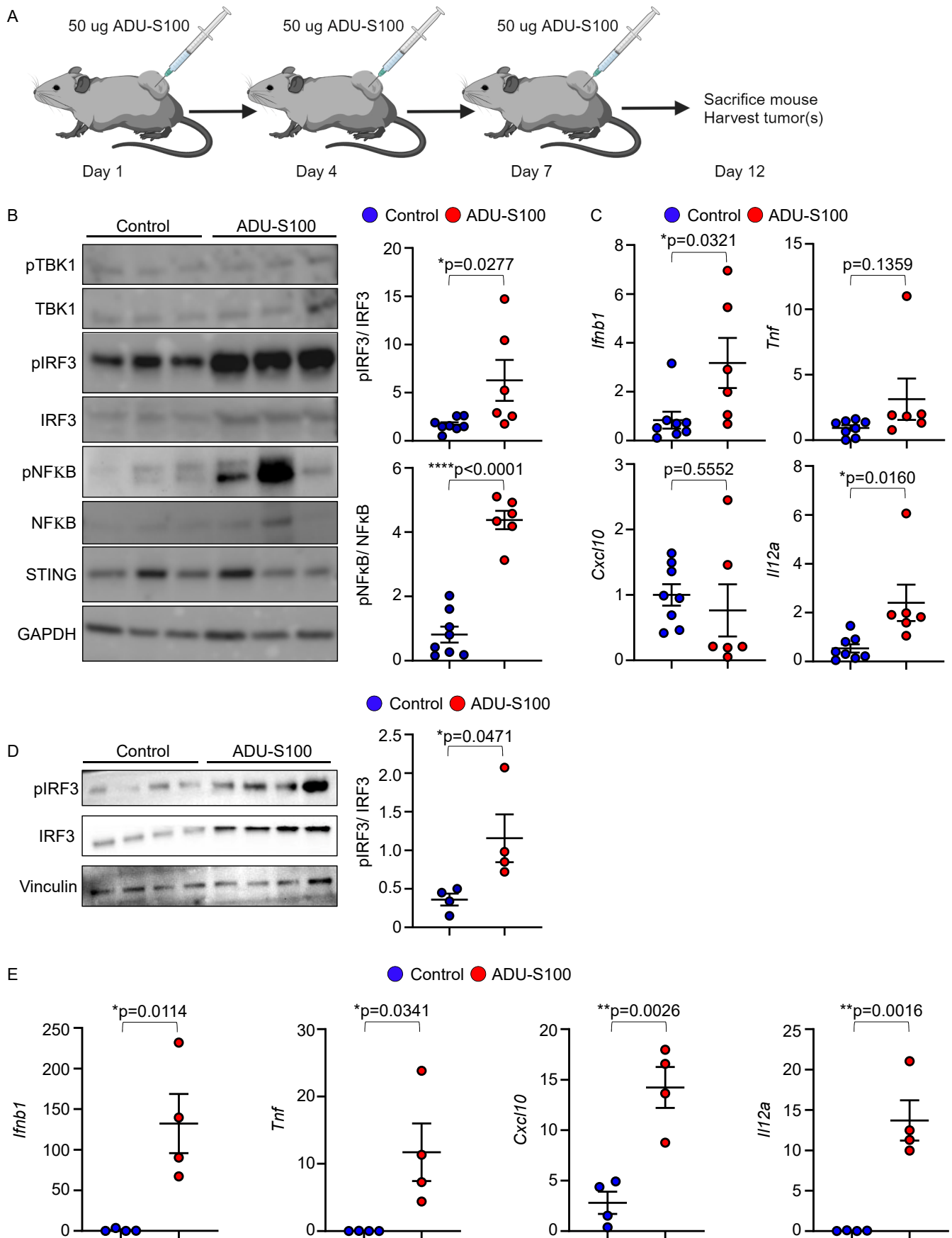


Figure 2. ADU-S100 treatment of *cisNP* mice activates the STING pathway in tumors.

(A) Schema of ADU-S100 treatment protocol. (B) Western blot analysis for expression of the indicated proteins in MPNSTs harvested from *cisNP* mice treated with vehicle control (n=8) or ADU-S100 (n=6). Quantified protein band intensities are shown graphically on the right. (C) PCR analysis of fold change in cytokine gene expression (*Ifnb1*, *Tnf*, *Cxcl10*, and *Il12a*) in *cis*MPNSTs harvested from control-treated (n=8) and ADU-S100-treated (n=6) mice. (D) Western blot analysis for expression of the indicated proteins in MPNSTs harvested from *cisNP* mice treated with vehicle control (n=4) or ADU-S100 (n=4) for 24 hours. Quantified protein band intensities are shown graphically on the right. (E) PCR analysis of fold change in cytokine gene expression (*Ifnb1*, *Tnf*, *Cxcl10*, and *Il12a*) in *cis*MPNSTs harvested from control-treated (n=4) and ADU-S100-treated (n=4) mice 24 hours after treatment. Data are represented as mean \pm SEM and p values are determined by two-tailed t test with respect to vehicle control. * $P < 0.05$, ** $P < 0.01$, **** $P < 0.0001$. Scale bar: 50 μ m.

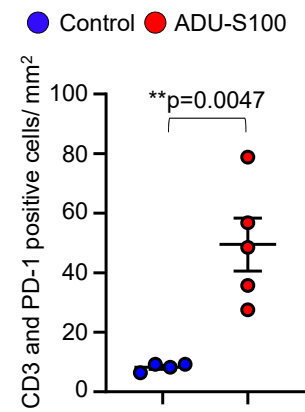
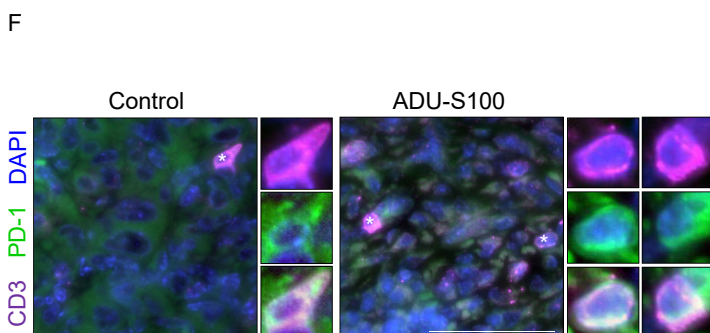
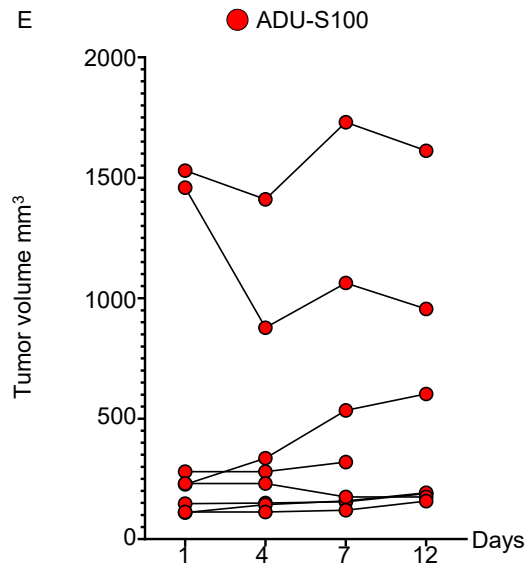
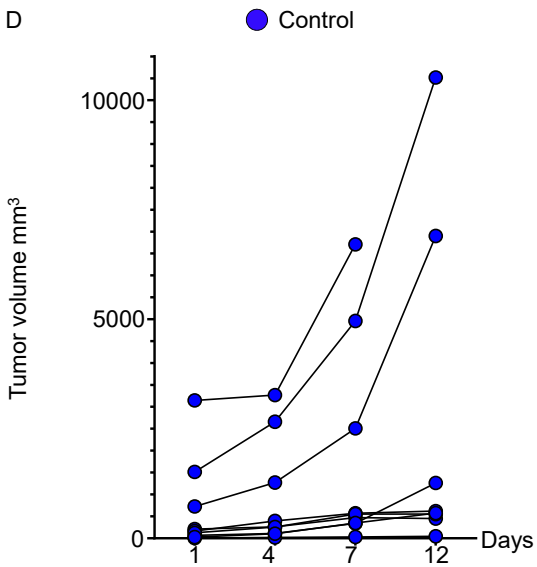
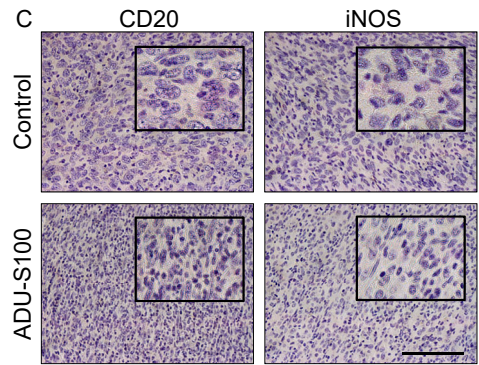
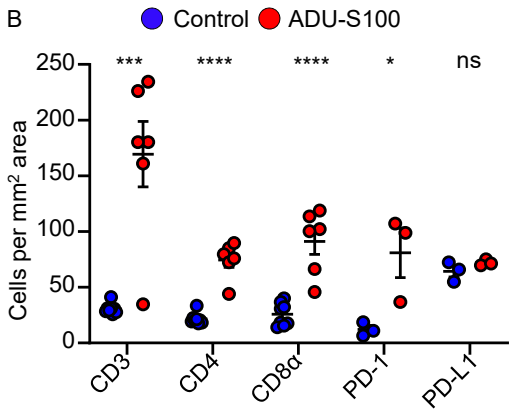
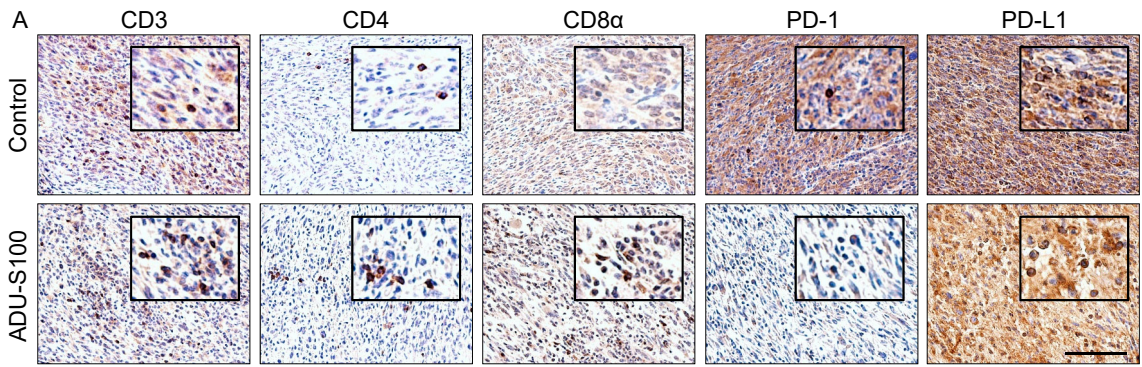


Figure 3. STING activation in MPNST increases T cell infiltration and impedes tumor growth.

(A) Paraffin sections of MPNSTs harvested from vehicle-treated or ADU-S100 treated *cisNP* mice were stained with antibodies against CD3, CD4, CD8 α , PD-1, and PD-L1 and quantified (B). (C) The same sections were also stained for CD20 and iNOS. (D-E) Tumor volume change with time in response to indicated treatments. (F) Co-immunostaining for CD3 and PD-1 (left) with quantification (right). Cells marked with asterisks in each panel are magnified and shown adjacently. Control, n=4; ADU-S100, n=5. Scale bar: 50 μ m. Data are represented as mean \pm SEM and p values are determined by unpaired t test with respect to vehicle control. * $P < 0.05$, ** $P < 0.01$, *** $P < 0.001$, **** $P < 0.0001$, ns = not significant. See Materials and Methods for a detailed description on staining methodology.

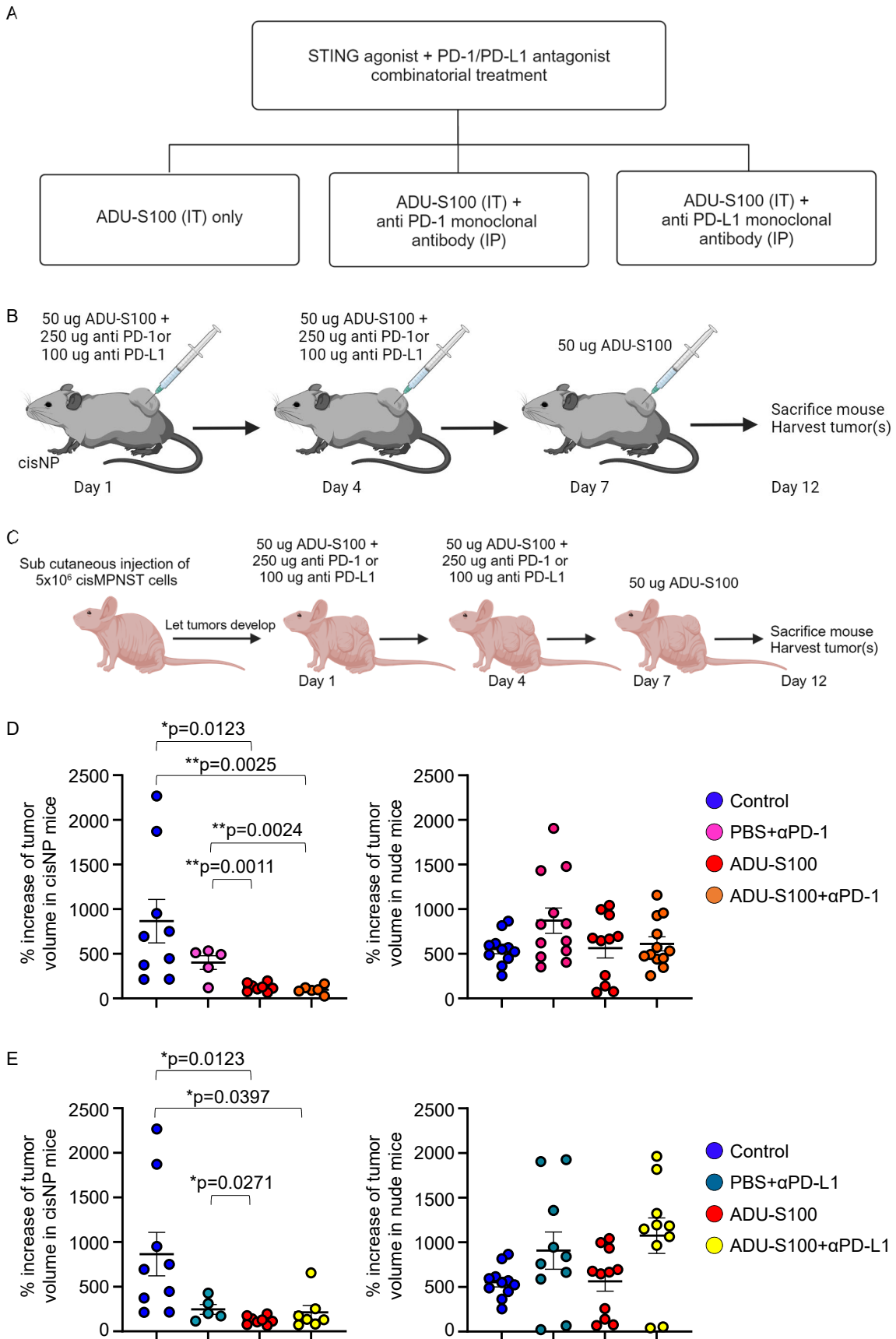


Figure 4. Combination treatment of *cisNP* mice with STING agonist plus ICB delays tumor growth.

(A) Treatment arms for STING activation followed by ICB study. (B) Schema of drug treatment for STING activation and ICB in *cisNP* mice. (C) Schema of STING activation and ICB in nude mice. (D-E) Percent increase in tumor volume in *cisNP* mice and in nude mice with the indicated treatments. Control, n=9; ADU-S100, ADU-S100 + α PD-1, n=6; PBS + α PD-1, n=6, PBS + α PD-L1, n=5, ADU-S100 + α PD-L1, n=7 for *cisNP* mice. Control, n=11; ADU-S100, n=11; ADU-S100 + α PD-1, n=12; PBS + α PD-1, n=12, PBS + α PD-L1, n=10, ADU-S100 + α PD-L1, n=10 for nude mice. The same data sets for control and ADU-S100 treatments in panel (D) are shown in the respective graphs in panel (E) for clarity and ease of comparison. Data are represented as mean \pm SEM and p values are determined by Tukey's multiple comparisons test as indicated. * $P < 0.05$, ** $P < 0.01$.

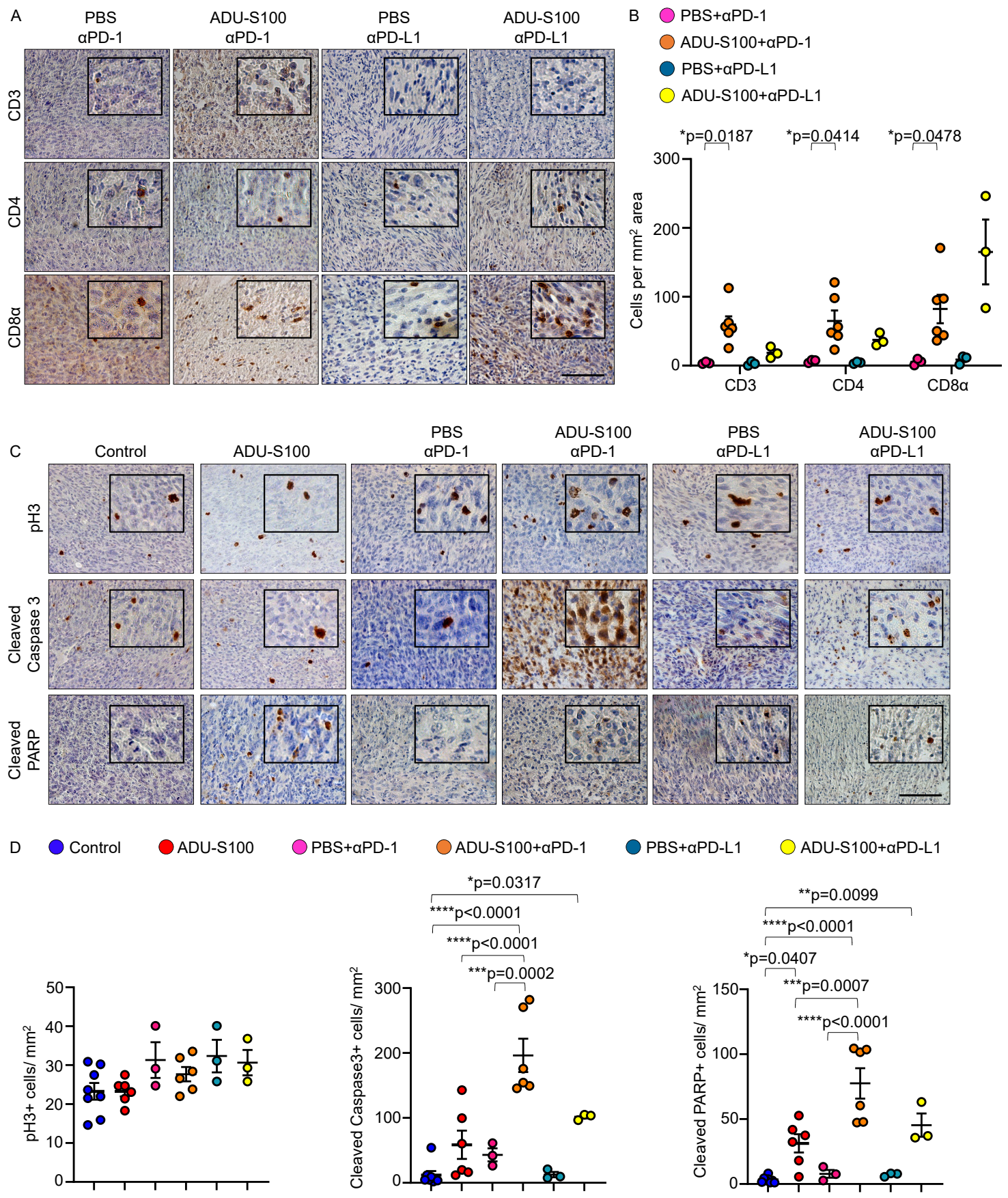
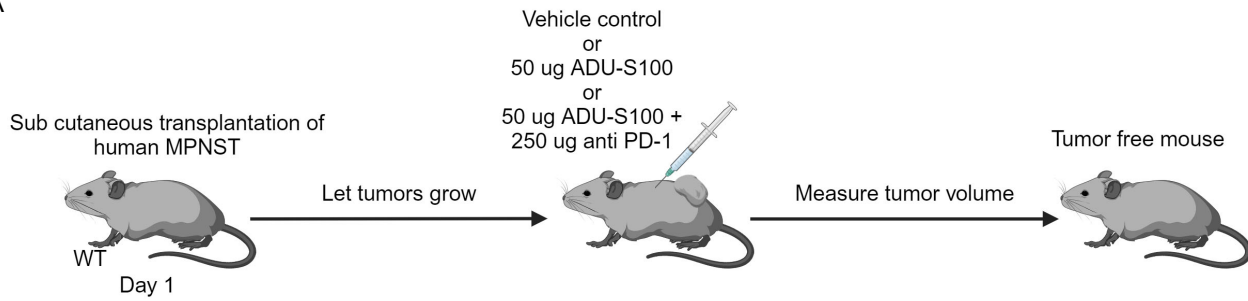


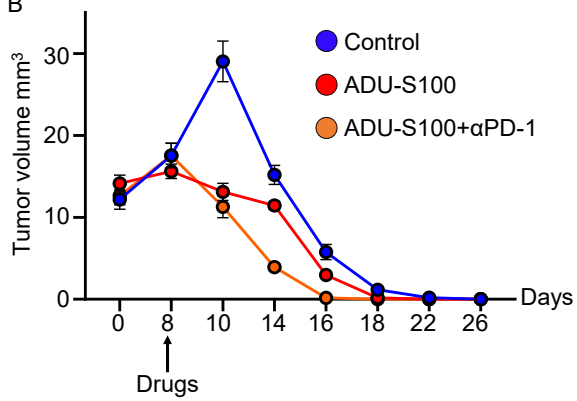
Figure 5. Combination treatment of *cisNP* mice with STING agonist plus ICB increases expression of apoptotic markers in MPNSTs.

(A) Paraffin sections from MPNSTs harvested from mice treated as indicated were stained for T cell markers. (B) Quantification of images in (A). (C) Paraffin sections from MPNSTs harvested from mice treated as indicated were stained for phospho-H3 (pH3), Cleaved Caspase 3, and Cleaved PARP. (D) Quantification of pH3-positive cells (left), Cleaved Caspase 3-positive cells (middle), and Cleaved PARP-positive cells (right) in tumors treated as indicated in (C). Control, n=8; ADU-S100, ADU-S100 + α PD-1, n=6; PBS + α PD-1, PBS + α PD-L1, ADU-S100 + α PD-L1, n=3. Data are represented as mean \pm SEM and p values are determined by two-tailed t test in (B) and Tukey's multiple comparisons test in (D) as indicated. * $P < 0.05$, ** $P < 0.01$, *** $P < 0.001$, **** $P < 0.0001$. Scale bar: 50 μ m. See Materials and methods for a detailed description on staining methodology.

A

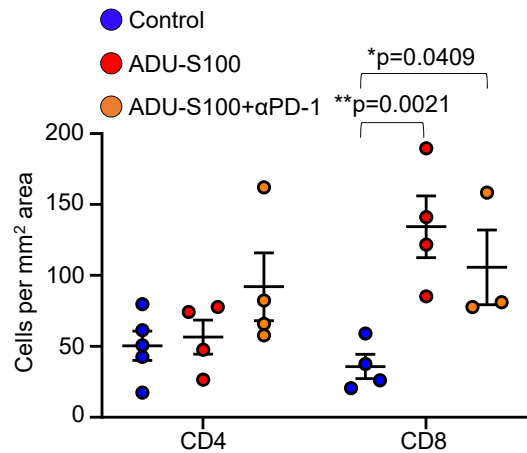
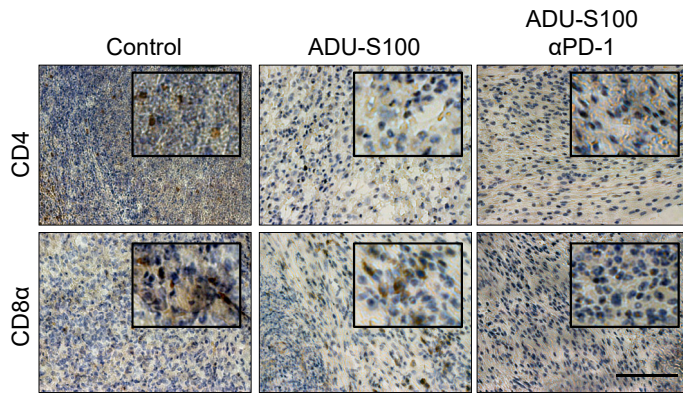


B



	Control vs ADU-S100	Control vs ADU-S100 + αPD-1	ADU-S100 vs ADU-S100 + αPD-1
Day 10	p<0.000001	p<0.000001	ns
Day 14	p=0.003491	p<0.000001	p<0.000001
Day 16	p=0.00562	p<0.000001	p<0.000001
Day 18	p=0.000491	p=0.00006	ns
Day 22	p=0.001019	p=0.000104	ns
Day 26	ns	ns	ns

C



D

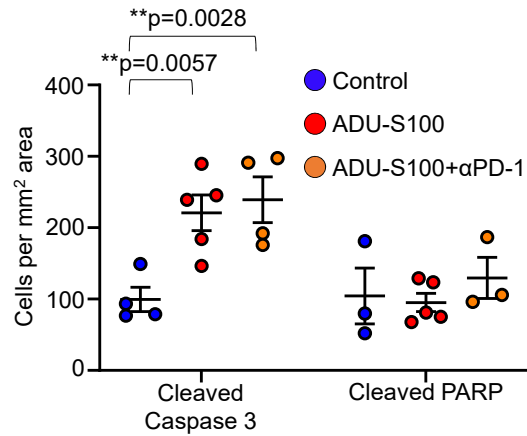
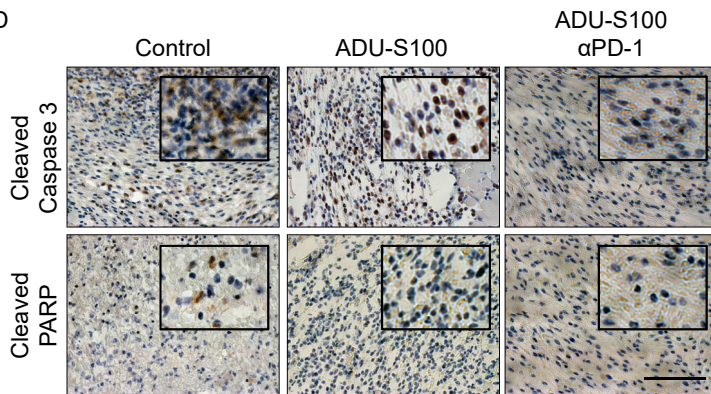


Figure 6. Combination treatment of xenograft human MPNST with STING agonist plus ICB accelerates complete tumor regression.

(A) Schema for designing the mouse xenograft MPNST model and the treatment regimen with ADU-S100 and ICB. (B) Volume change of xenograft MPNST upon the indicated treatments. Control, ADU-S100, and ADU-S100 + α PD-1; n=15. (C) Paraffin sections from xenograft MPNST treated as indicated were stained for T cell markers. (D) Paraffin sections from xenograft MPNST treated as indicated were stained for Cleaved Caspase 3 and Cleaved PARP. Control, n=3-4; ADU-S100, n=3-4; ADU-S100 + α PD-1, n=3-4. Data are represented as mean \pm SEM and p values are determined by Tukey's multiple comparisons test as indicated. * $P < 0.05$, ** $P < 0.01$. Scale bar: 50 μ m.

Table 1: Drug doses, routes of administration, and dosing schedule

Mouse MPNST Model	Treatment	Dose	Administration	Dosing Schedule
<i>cisNP</i>	PBS (vehicle for ADU-S100)		Intratumoral	Day 1, 4, 7; harvest Day 12
<i>cisNP</i>	ADU-S100	50 µg	Intratumoral	Day 1, 4, 7; harvest Day 12
<i>cisNP</i>	PBS + αPD-1	250 µg	Intratumoral Intraperitoneal	Day 1, 4, 7; harvest Day 12 Day 1, 4
<i>cisNP</i>	PBS + αPD-L1	100 µg	Intratumoral Intraperitoneal	Day 1, 4, 7; harvest Day 12 Day 1, 4
<i>cisNP</i>	ADU-S100 + αPD-1	50 µg + 250 µg	Intratumoral Intraperitoneal	Day 1, 4, 7; harvest Day 12 Day 1, 4
<i>cisNP</i>	ADU-S100 + αPD-L1	50 µg + 250 µg	Intratumoral Intraperitoneal	Day 1, 4, 7; harvest Day 12 Day 1, 4
<i>cisNP</i>	ADU-S100 + αPD-1 + αCTLA-4	50 µg + 250 µg + 300 µg	Intratumoral Intraperitoneal Intratumoral	Day 1, 4, 7; harvest Day 12 Day 1, 4 Day 1, 4
<i>cisNP</i>	ADU-S100 + αCTLA-4	50 µg + 300 µg	Intratumoral Intratumoral	Day 1, 4, 7; harvest Day 12 Day 1, 4
<i>cisNP</i>	PBS (vehicle for SA3)		Intraperitoneal	Day 1; harvest Day 12
<i>cisNP</i>	SA3	50 mg/ kg	Intraperitoneal	Day 1; harvest Day 12
Conditional MPNST	ADU-S100	50 µg	Intratumoral	Day 1, 4, 7; harvest Day 12
Conditional MPNST	PBS + αPD-1	250 µg	Intratumoral Intraperitoneal	Day 1, 4, 7; harvest Day 12 Day 1, 4
Conditional MPNST	ADU-S100 + αPD-1	50 µg + 250 µg	Intratumoral Intraperitoneal	Day 1, 4, 7; harvest Day 12 Day 1, 4
Conditional MPNST	PBS (vehicle for ADU-S100)		ADU-S100 + αPD-1	Day 1, 4, 7; harvest Day 12
Xenograft MPNST	PBS (vehicle for ADU-S100)		Intratumoral	Day 1, 4, 7; harvest Day 12
Xenograft MPNST	ADU-S100	50 µg	Intratumoral	Day 1, 4, 7; harvest Day 12
Xenograft MPNST	ADU-S100 + αPD-1	50 µg + 250 µg	Intratumoral Intraperitoneal	Day 1, 4, 7; harvest Day 12 Day 1, 4